JOURNAL OF THE ROYAL SOCIETY Interface

Vortex wakes generated by robins *Erithacus rubecula* during free flight in a wind tunnel

A Hedenström, M Rosén and G.R Spedding

J. R. Soc. Interface 2006 **3**, 263-276
doi: 10.1098/rsif.2005.0091

JOURNAL OF THE ROYAL SOCIETY Interface

J. R. Soc. Interface (2006) **3**, 263–276
doi:10.1098/rsif.2005.0091
Published online 13 October 2005

Vortex wakes generated by robins *Erithacus rubecula* during free flight in a wind tunnel

A. Hedenström[1,*], M. Rosén[2] and G. R. Spedding[3]

[1]*Department of Theoretical Ecology, Lund University, Ecology Building, 223 62 Lund, Sweden*
[2]*Department of Animal Ecology, Lund University, Ecology Building, 223 62 Lund, Sweden*
[3]*Department of Aerospace and Mechanical Engineering, University of Southern California, Los Angeles, CA 90089-1191, USA*

The wakes of two individual robins were measured in digital particle image velocimetry (DPIV) experiments conducted in the Lund wind tunnel. Wake measurements were compared with each other, and with previous studies in the same facility. There was no significant individual variation in any of the measured quantities. Qualitatively, the wake structure and its gradual variation with flight speed were exactly as previously measured for the thrush nightingale. A procedure that accounts for the disparate sources of circulation spread over the complex wake structure nevertheless can account for the vertical momentum flux required to support the weight, and an example calculation is given for estimating drag from the components of horizontal momentum flux (whose net value is zero). The measured circulations of the largest structures in the wake can be predicted quite well by simple models, and expressions are given to predict these and other measurable quantities in future bird flight experiments.

Keywords: aerodynamics; wake; force balance; flight; digital particle image velocimetry; *Erithacus rubecula*

1. INTRODUCTION

A flying animal generates a periodic wake that contains the total impulse associated with the aerodynamic force developed by the wings, tail and body. In wakes that are dominated by vortical flows, rather than simply accelerated potential flows, the topology and quantitative properties of the vortices in the wake can be used to determine the direction and magnitude of the aerodynamic forces on the wings and body; in a sense they are the aerodynamic foot print of the flying animal. Analysis of the vortex wake is convenient since the measurements are non-intrusive and direct comparisons are possible with a set of aerodynamic models that are explicitly based on presumed wake topology (Rayner 1979*a*,*b*; Pennycuick 1989*a*; Spedding 1992).

A custom digital particle image velocimetry (DPIV) method was recently deployed for recording bird wakes in a wind tunnel (Spedding *et al.* 2003*a*), and subsequently used to investigate wake properties across the natural flight speed range (4–10 m s^{-1}) of a 30 g thrush nightingale *Luscina luscina* (Spedding *et al.* 2003*b*). The main findings were that wake topology and quantitative properties (vorticity, circulation) change continuously from slow to fast flight speed, without any discontinuities that would have indicated discrete 'gaits'. The wake structure appeared to be more complicated than idealized models involving a mixture of positive (anti-clockwise) and negative (clockwise) vorticity shed near the transition between down- and upstroke. A careful book-keeping of vorticity shed during an entire wing beat did, however, result in an approximate force balance between downward momentum flux and weight. A simple empirical vortex wake-based aerodynamic model (the ER model) was constructed, based on these findings. A companion paper (Rosén *et al.* 2004) described the wing beat kinematics of the same bird in the same flight conditions and the wake geometry was related to the observed kinematics.

Even though these conclusions were based on a very extensive data set the results all came from a single bird. The success and quality of such studies depend on repeatable behaviour of birds trained to fly in a wind tunnel, which is quite difficult to achieve, particularly, with more than one or two individuals. It is nevertheless important to investigate not only other species, but also more than one individual of one species, to check the generality and repeatability of the results. Here we present wake data from two robins *Erithacus rubecula*, which is a migratory songbird species of about half the body mass of the thrush nightingale. The experimental

*Author for correspondence (anders.hedenstrom@teorekol.lu.se).

Received 29 June 2005
Accepted 8 September 2005

procedures and analysis methods will combine and follow those described in Spedding *et al.* (2003*b*) and Rosén *et al.* (2004).

2. MATERIAL AND METHODS

2.1. Wind tunnel, birds and training

The birds were trained to fly in the front half of the test section in a wind tunnel designed specifically for bird flight experiments (detailed technical specifications, including extensive mean turbulence measurements can be found in Pennycuick *et al.* 1997). Birds were trained to sit on a movable perch in the centre of the test section. When the perch was lowered, the birds would start to fly. To help birds fly at the same location a visual light marker was inserted upstream of the test section, but out of the image plane to avoid disturbing the measurements. The lighting is otherwise dimmed (a requirement for DPIV images) so the marker is easily the brightest visual reference point. When the bird flew steadily in the desired location the laser was allowed to flash and shortly after the perch was elevated to allow the bird to land. In this way, a reward (landing on the perch) was generated shortly after the bird flew steadily in the desired location, conditioned by the flashing laser light. The speed range where the birds would fly steadily was 4–9 $\mathrm{m\,s^{-1}}$, and data were obtained at each integer speed in this range for bird#1, and at speeds 4, 6, 8 and 9 $\mathrm{m\,s^{-1}}$ for bird#2. All speeds refer to the equivalent airspeed defined as

$$U_{\mathrm{e}} = \sqrt{2q/\rho_0},$$

where ρ_0 is the assumed value for the air density at sea level in the International Standard Atmosphere (1.255 $\mathrm{kg\,m^{-3}}$), q ($=\rho U^2/2$) is the dynamic pressure and ρ is the measured air density during an experiment. Henceforth, we will use U for short. In all experiments, the air density (ρ) was 1.18–1.22 $\mathrm{kg\,m^{-3}}$, and temperature was 19–21 °C. Morphological data for the two robins and derived aerodynamic measures are given in table 1. Wing semi-span is half the full wing span as measured on the bird on fully outstretched wings. The wing area includes the area of the body between the wings and was measured according to the method recommended by Pennycuick (1989*b*). The Reynolds number ($Re=Uc/\nu$, where c is the mean chord length of the wing and ν is the kinematic viscosity) ranged from $Re=13\,200$ at $U=4\ \mathrm{m\,s^{-1}}$ to $Re=29\,800$ at $U=9\ \mathrm{m\,s^{-1}}$. Since the bird is small in comparison with the test section, interactions with the side walls were ignored.

2.2. Wing kinematics

Kinematic measurements were conducted following the procedures laid out in Rosén *et al.* (2004). Frame sequences were obtained from digital video recordings using a Redlake MotionScope PCI500, operating at a frame rate of 250 $\mathrm{s^{-1}}$ and shutter speed 1/1850 s, shooting from a rear view 4 m downstream from the bird's flight position. The camera was placed far back in the first diffuser where it causes negligible effects on the airflow in the test section (Pennycuick *et al.* 1997). The wingtips and shoulder joints were digitized for stable flight sequences, from which wingbeat period and frequency ($T=1/f$), downstroke fraction (τ; downstroke duration divided by T), span ratio (R; wing span at mid upstroke divided by wing span at mid downstroke), and wing tip peak–peak amplitude (A) were derived. The reduced frequency, $k=\omega c/2U$, where $\omega=2\pi f$ is the angular frequency, may be used as an indicator of the relative importance of unsteady terms in the aerodynamics. As a rough guide, values of $k\approx1$ suggest a likely significant contribution from time-varying flow, while $k\approx0.1$ indicates that it can be ignored (Spedding 1992).

Table 1. Morphological data of the two robins used for wind tunnel flight experiments.

measure	symbol	units	bird#1	bird#2
semi-span	b	cm	11.0	11.3
wing area	S	$\mathrm{cm^2}$	103.8	104.0
mean chord	c	cm	4.7	4.6
aspect ratio	AR		4.7	4.9
body mass	m	g	16.75	16.31
wing loading	Q	$\mathrm{N\,m^{-2}}$	15.8	15.4

2.3. Flow visualization

The DPIV technique used for flow visualization has been described in detail elsewhere (Spedding *et al.* 2003*a*). The re-circulating tunnel is filled with a thin fog (particle size 1 μm), illuminated by a double-pulsed laser (Spectra Physics Quanta Ray PIV II, dual head Nd : YAG) generating green light (532 nm). A sequence of lenses and mirrors generates a thin (3 mm) vertical light sheet aligned with the flow. The laser produces pulse pairs at a rate of 10 Hz, where the time between the two pulses, δt, can be set arbitrarily and accurately by a Stanford Research Systems DG535 delay generator. All data here were collected with $\delta t=400$ μs. The centre of the light sheet is approximately 0.8 m downstream of the bird, separated by a grid of infrared LED-photodiodes arranged so that if any beam is intercepted by the bird, laser pulses are suspended immediately.

An independent video camera positioned in the first diffuser downstream from the test section monitored the position of the bird in relation to the light sheet. In the rear view the light sheet appears as a vertical rod with the bird flying in front of it clearly visible. The position of the light sheet with respect to the wing span at mid downstroke was coded as follows: left wing=l, right wing=r, mid-wingspan or body, henceforth termed centre plane (lr), inner wing (x), outer wing (y) and wing tip (z). For example, a record from the left outer wing is coded 'ly'. Most data presented in this paper are from the centre plane position, directly downstream of the body.

2.4. DPIV analysis

The two laser pulses were imaged onto two Pulnix TM9701N full frame transfer CCD array cameras, in upstream–downstream sequence. Flow fields were derived from coupled image pairs, using the correlation imaging velocimetry (CIV) technique of Fincham & Spedding (1997). The value of $\delta t = 400$ μs was selected to obtain a mean maximum displacement of 5 pixels between consecutive images, in which case the velocity band width is 1 : 100, and the uncertainty in velocity estimation is approximately ±1% (Spedding *et al.* 2003*a*). The residual (the part not automatically removed by the dual camera sequence) mean flow was removed from wake images so that the computed flow fields measure the bird disturbances only. The velocity components u, v and w are defined in the streamwise (x), spanwise (y) and vertical (z) directions. Because of the streamwise vertical alignment of the image plane, the spanwise component of vorticity (normal to the image plane) could be calculated as

$$\omega_y = \frac{\partial w}{\partial x} - \frac{\partial u}{\partial z}. \tag{2.1}$$

ω_y is calculated from a smoothed spline interpolation of the velocity field. It is calculated directly from the spline coefficients and not from a finite difference approximation. The most likely uncertainty in ω_y is ±10%.

The strength of a vortex structure is measured by its circulation

$$\Gamma = \int_S \omega_y \, \mathrm{d}S, \tag{2.2}$$

where ω_y is integrated over the area S required to cover all regions of non-zero ω_y. In practice, Γ was estimated using a discrete approximation of equation (2.2) as

$$\Gamma = \sum_i \sum_j \omega_y(i,j) \mathrm{d}x \, \mathrm{d}y, \tag{2.3}$$

where the summation was calculated from all contiguous cells (i, j) where ω_y exceeds 20% of its peak value. The 20% threshold is chosen to ensure that all qualifying cells come from estimates that are significantly above background noise. Any thresholding procedure is guaranteed to underestimate Γ, but the estimate was compensated by adding back the presumed sub-threshold tails of the distribution, assuming each blob was Gaussian in form. The vorticity and circulation were computed for all main vortex structures in wake data sorted by speed and wing position.

The normalized peak vorticity is given by $\Omega = |\omega_y|_{\max} c/U$, and measures from positive and negative-signed vortices are denoted Ω^+ and Ω^- respectively, while their corresponding normalized circulations, Γ/Uc, are denoted Γ^+ and Γ^-. In all figures, the symbols show mean values, ±1 s.d.

2.5. Force balance

The net aerodynamic force must balance weight and drag in steady level flight. To evaluate the quantitative wake data, we can construct the simplest possible wake model composed of periodic bursts of vertical momentum. Following the ideas of Rayner (1979*a*), let us suppose that the wake consists of elliptical vortex loops shed only during the downstroke. The vertical impulse, I_z, of each loop is given by the product of the projected area, S_e, of the vortex loop onto the horizontal plane and the circulation

$$I_z = \rho S_e \Gamma_1. \tag{2.4}$$

Again, for simplicity, we will assume that the ellipse geometry is completely determined by the kinematics in the flightwise direction and by the wingspan in the spanwise direction, ignoring all corrections for span efficiency. Thus, the area of the elliptic loop is determined by the downstroke wake wavelength $\lambda_d = UT\tau$, where T is stroke period and τ is downstroke fraction, and the wing semispan, b, as

$$S_e = \pi b(\lambda_d/2). \tag{2.5}$$

In steady level flight the weight, $W = mg$, is balanced by the average impulse per unit time, and so the total impulse associated with downstroke-generated momentum flux must cover the entire stroke period, T. Therefore, we may write

$$W = \frac{I}{T} = \frac{\rho S_e \Gamma_1}{T}, \tag{2.6}$$

thus identifying a reference circulation, Γ_1, which is the average circulation required to support the weight, if the wake consists of discrete elliptical vortex loops shed from the downstroke. Equation (2.6) can be re-arranged to solve for Γ_1:

$$\Gamma_1 = WT/\rho S_e. \tag{2.7}$$

Alternatively, if the wake were imagined to consist of straight trailing wing-tip vortices, like an idealized wake in steady gliding flight, the circulation required to support the weight would be determined by the size of the rectangular area mapped out during one (infinitesimal amplitude) wingbeat. Following the argument of equations (2.6) and (2.7), a second, 'power-glider' reference circulation can be written

$$\Gamma_0 = W/\rho U 2b. \tag{2.8}$$

Although the simplifications are extreme, the two reference circulations mark two convenient (idealized) limits of powered flight with pulsed loops and continuous trailing wakes. They are related by the ratio of their vertically projected wake areas as $\Gamma_0 = \Gamma_1 S_e/UT2b$, as noted in Spedding *et al.* (2003*b*).

3. RESULTS

3.1. Wake topology

Each individual frame/velocity field covers about two-third of the extent of the periodic wake in the flightwise direction. The sampling rate of 10 Hz is smaller than the 14 Hz wingbeat frequency, so traces from consecutive wingbeats are sampled at a different phase in each frame. These phase-shifted sequential fields are then assembled so that repeated structures overlap, and together form a view of the wake over one or more wingbeats. The periodic wake structures can quickly be

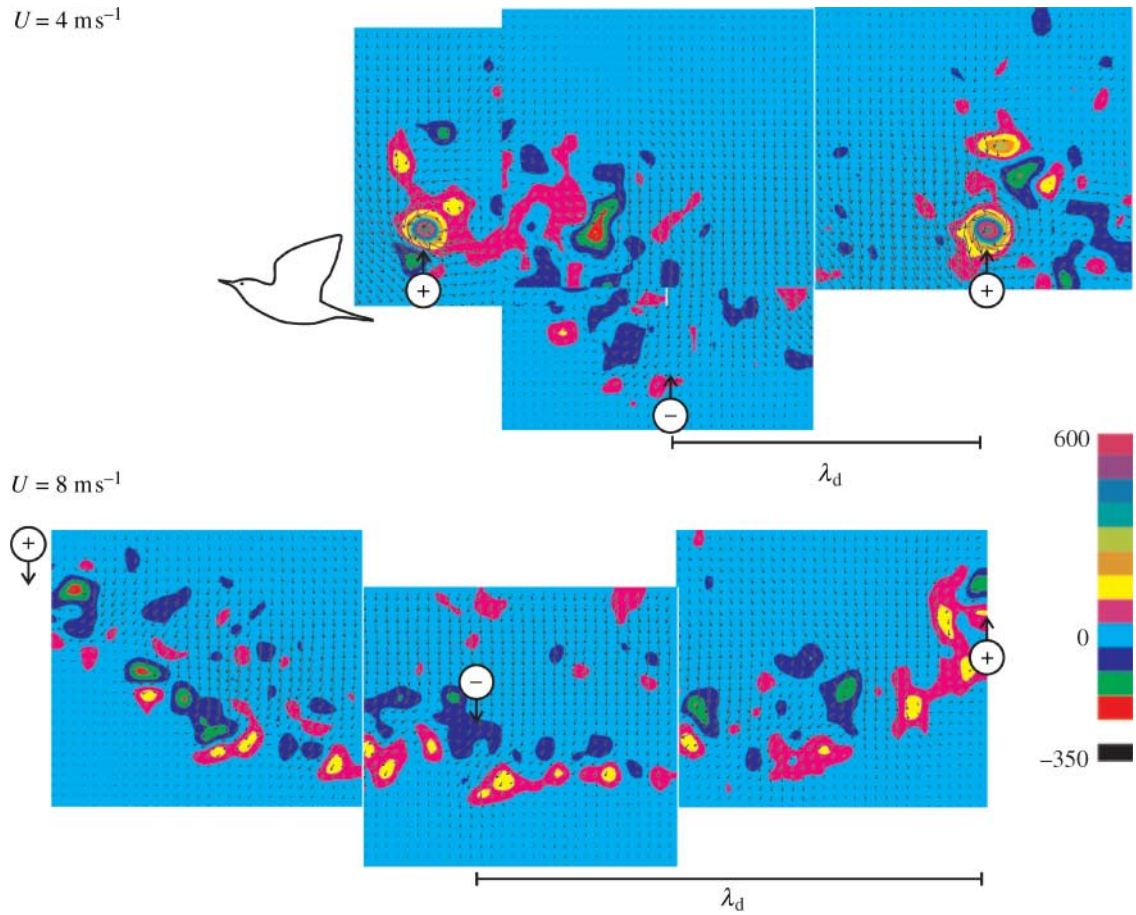

Figure 1. Composite colour-coded spanwise vorticity fields, $\omega_y(x, z)$, with velocity vectors superimposed at half their true spatial resolution for flight speeds $U=4$ and 8 m s^{-1}. Data are from the vertical centreplane. The vorticity is mapped asymmetrically about a 14-step colour bar to local extrema of -350 and 600 s^{-1}. The resolution of the colour bar matches the worst-case uncertainty in the measurements so that visible features are likely to exist. Regions corresponding to start and stop vortices are indicated by (+) and (−) arrows. At $U=4$ m s^{-1} (wake wavelength, $\lambda \cong 0.29$ m), the stop vortices can be barely measurable, and instead a diffuse trail of vorticity marks the upstroke. At $U=8$ m s^{-1} ($\lambda \cong 0.57$ m) the entire wake is composed of trails of weak transverse vorticity only. The figure shows the downstroke wavelength λ_d for each speed. The vorticity fields have been combined from consecutive frames in a sequence, starting from right to left, with the bird flying towards left as indicated by bird silhouette. Data are from bird#1, but bird#2 shows the same patterns.

recognized and their location in the overall pattern is simple to find because, when the bird flies from right to left, wake segments generated during downstroke motions trail from top right to bottom left of the field of view, while those coming from the upstroke follow a line from bottom right to top left. When the wake traces appear with constant phase-shift and at the same vertical position, a criterion can be set for determining that this particular flight segment is steady and level. This is done independently of the downstream camera information, which is then used to corroborate.

Since the wings accelerate/decelerate most rapidly at the beginning and end of each wingstroke, then it is reasonable to look for large vortex structures left behind in the wake at these points. We will term the largest patch of positively signed vorticity formed at the beginning of the downstroke a 'start vortex', and the corresponding patch of vorticity (of opposite sign) left at the end of the downstroke will be termed a 'stop vortex'. This notational convenience is informed by previous similar wake studies, and is for labelling only. Here, as in previous studies, it will become apparent that the wake structure is significantly more complicated than can be expressed through cross-sections through pairs of 'start–stop' vortices. However, their position, spatial distribution and strength are still useful markers and diagnostics of the global wake.

Wake reconstructions and quantitative surveys were performed for all flight speeds from 4–9 m s^{-1}, and at all spanwise locations. Figure 1 shows two examples only from this extensive grid of data. A total of 1198 frames for bird#1 and 828 for bird#2 fulfilled the criteria for inclusion in the analysis. These data were distributed quite evenly across flight speeds and wing positions.

At slow speed ($U=4$ m s^{-1}, figure 1), there are coherent and well-defined start vortices of positive (anti-clockwise rotation) circulation, while the cross-section of the associated stop vortex generally covers a larger area. Notice that the region of the stop vortex at the transition between down-/upstroke also contain patches of low amplitude positive vorticity embedded among the dominating patches of negative vorticity. The induced downwash, indicated by velocity vectors, is strongest between start and stop vortex cores. The

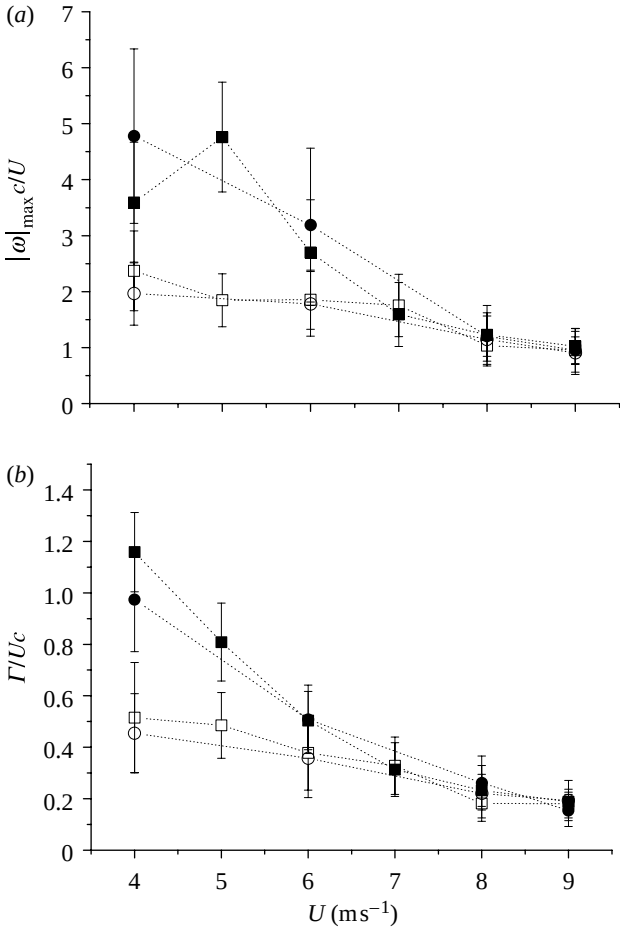

Figure 2. Variation in peak vorticity magnitude $|\omega_y|_{\max} c/U$ (*a*) and measured circulation of the strongest starting (filled symbols) and stopping (open symbols) vortices Γ/Uc (*b*), rescaled by the mean wing chord c and mean speed U, as a function of flight speed U. The symbols represent mean$\pm$1 s.d. for bird#1 (squares) and bird#2 (circles), respectively. Sample sizes are (starting vortex, stopping vortex): (28, 16), (66, 55), (44, 43), (27, 40), (27, 40), (10, 18) for bird#1 at U=4–9 m s^{-1}, and (15, 15), (30, 33), (32, 46), (17, 32) for bird#2 at U=4, 6, 8 and 9 m s^{-1}, respectively.

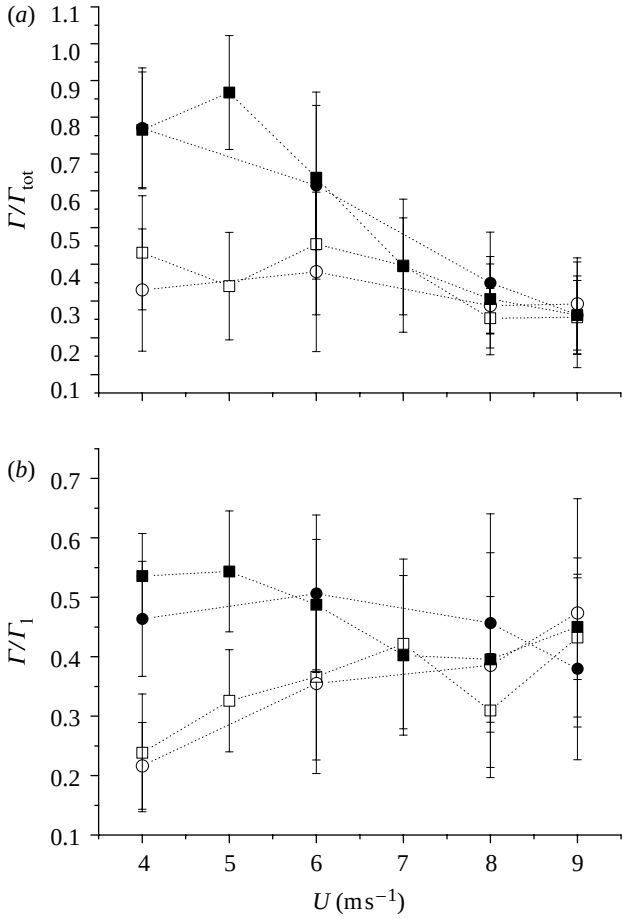

Figure 3. Variation in circulation of the strongest starting (filled symbol) and stopping (open symbol) vortices as a ratio of the total same-signed vorticity in the same image (*a*), and as a ratio of the reference circulation Γ_1 required to support the weight by downstroke generated vortex loops (*b*), as a function of flight speed for bird#1 (squares) and bird#2 (circles). Symbols represent mean$\pm$1 s.d. Sample size as for figure 2.

vorticity pattern of figure 1*a* comes from the centre-plane position, where the horizontal distance between start and stop vortex cores should reflect the wavelength of the wingbeat as it is mapped onto the flight path.

At a higher speed (U=8 m s^{-1}, figure 1) the wake consists of a more continuous shedding of low amplitude vorticity of both signs. This uninterrupted wake trail is consistent with a more continuous production of aerodynamic forces throughout the wingbeat, in contrast with the more strongly pulsed nature of the slow speed wakes.

3.2. Quantitative wake properties

The normalized vorticity Ω^+ declines monotonically with increasing flight speed, U, (figure 2*a*). Peak Ω^- was about half of Ω^+ at slow speeds, but both Ω^+ and Ω^- converged to similar values $\approx$1 by U=7 m s^{-1} and thereafter remained similar. The same pattern was found for Γ^+ and Γ^- (figure 2*b*), with start vortices being stronger than stop vortices at U=4–6 m s^{-1}, and then converging to similar values for $U \geq 7$ m s^{-1}. There was no measurable difference between the two individual birds in either of these quantities, at any flight speed.

Differences in the spatial distribution of vorticity can be expressed as the fraction of circulation contained in the strongest vortex cross-section in relation to the total circulation of the same sign of the whole image. At slow speeds the majority of the positive-signed vorticity, and hence circulation, is confined to the strongest vortex, while the fraction outside the strongest vortex is much larger for negative vorticity (figure 3*a*). The fraction of the total positive vorticity contained within the strongest vortex declines with increasing flight speed, and by 7 m s^{-1} this fraction is the same for positive and negative vorticity.

3.3. Force balance

If the wake were to consist of idealized, discrete, elliptical vortex loops, then each one would be required to have a strength given by reference circulation Γ_1 (equation (2.7)) in order to provide weight support. The measured circulation is shown in figure 3*b*. If the

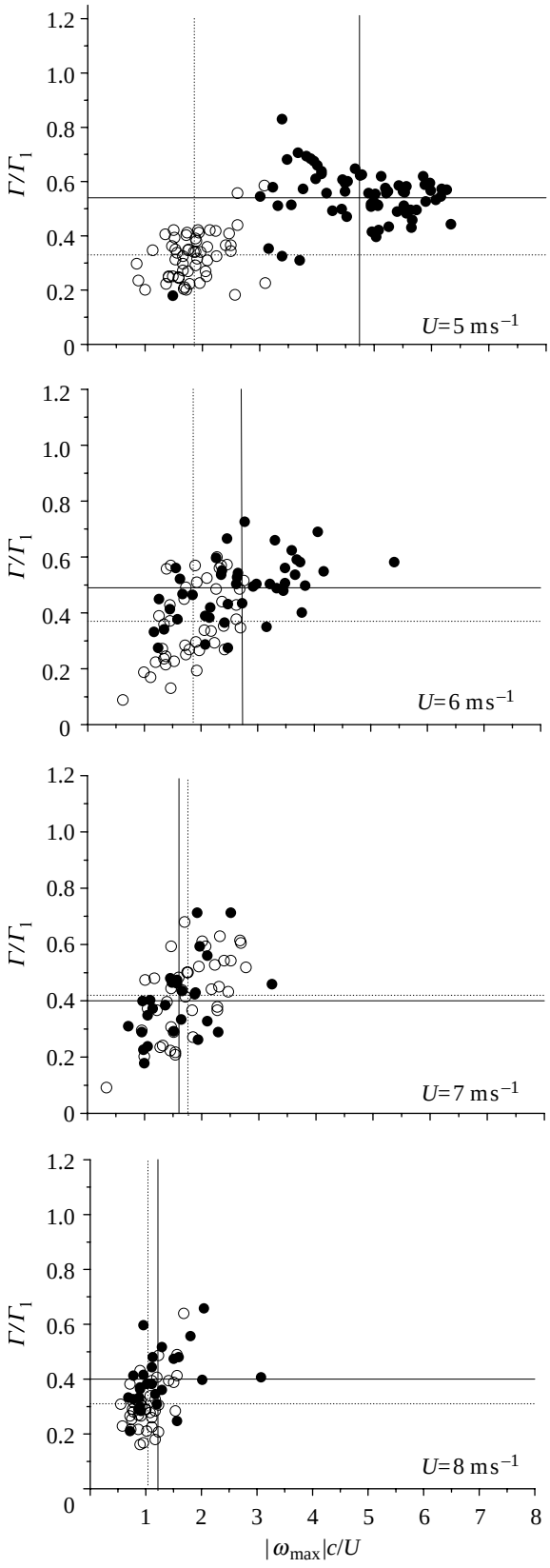

Figure 4. Normalized circulations and peak spanwise vorticity as a ratio of the reference circulation Γ_1 for starting (filled circles) and stopping (open circles) vortices, rescaled by the mean wing chord c and flight speed U for bird#1 at $U=5$, 6, 7, and 8 m s^{-1}. The solid horizontal and vertical lines represent means for starting vortices and the dotted lines are means for stopping vortices, and their intersections approximately mark the centroids of the measurement population. Sample sizes as for figure 2.

strongest start vortex represents all positive vorticity, its associated Γ/Γ_1 averages approximately 0.5 at $U=4$ m s^{-1} for the two robins. Hence, complete weight support is not achieved by an imagined sequence of closed-loop vortices, each one with uniform circulation given by the measured strength of start vortices. The strongest stop vortex contains, on average, even less circulation than the start vortices, with values of Γ/Γ_1 less than 0.25 at $U=4$ m s^{-1} increasing with increasing flight speed to about 0.45 at $U=9$ m s^{-1}.

Γ^+/Γ_1 declines with U, and is expected to do so because the wake topology increasingly differs from a simple closed loop. Since the spanwise vorticity appears as a continuous weak trail, the variations in bound circulation on the wing are likely to be smaller, and the streamwise, trailing vortices (with strengths comparable to the bound circulation) which are not measured, are likely to be much stronger than the relatively small increments in spanwise vorticity.

Figure 3*b* shows a decline in the measured strength of the vertical centreplane cross-section through the starting vortex, and a corresponding increase in strength of the stopping vortex. The points are averages, with quite large error bars and it is useful to see the population of measurements that comprise the average. Figure 4 shows the measured population of start and stop vortices in $\{\Gamma/\Gamma_1, \Omega\}$ space. The mean values of each measure are shown by solid and dashed lines for start and stop vortices, respectively. The two populations of vortices are quite distinct at $U=5$ m s^{-1}, clearly separable in $\{\Gamma/\Gamma_1, \Omega\}$. Although stop vortices are weaker, their distribution is more compact about the centroid. Start vortices have significantly higher Ω, but the variation in this axis is also high. As U increases, the two populations become increasingly similar, primarily through motion (in $\{\Gamma/\Gamma_1, \Omega\}$) of the start vortex population through decreases in both Γ/Γ_1 and Ω.

The start vortices contained approximately 50% of the circulation required to support the weight at $U=4$ m s^{-1}, and even less at higher flight speeds (figures 3*b* and 4). Accounting for the entire wake dynamics, therefore, requires a modification of the analysis or assumptions, or both. First, as figure 1 shows, at no speed is the wake left in the upstroke negligible. In Spedding *et al.* (2003*b*), the contribution to weight support of the upstroke was estimated by adding the vertical impulse generated from a rectangular wake section bounded by a line vortex of increasing strength as U increases. Second, the start and stop vortices of a single downstroke are usually surrounded by patches of opposite-signed vorticity, and these weak but broadly distributed fragments would not be counted anywhere if the accumulated circulation were taken only from the sign of the dominant vortex structure.

An approximate accounting for these modifications can be made by adding all remaining trace components associated with the downstroke, of either sign (denoted Γ^+_{tot} and Γ^-_{tot}), and then assuming that the wake impulse can be estimated from a downstroke elliptical loop with this combined strength. This assumption is reasonable at the very lowest flight speeds, but then will overestimate the total impulse because the projected wake area left by the upstroke is smaller than the

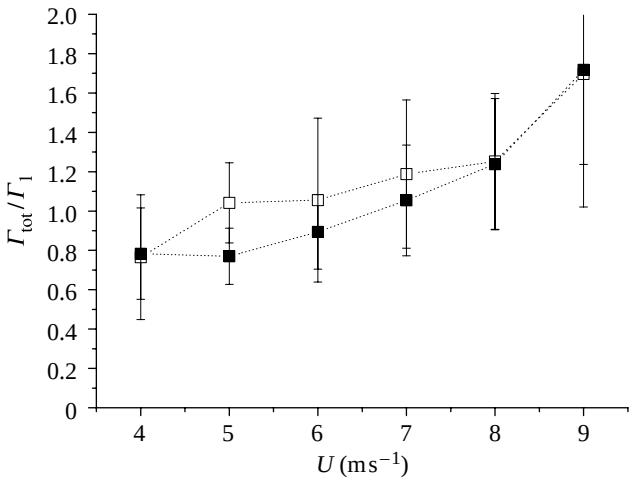

Figure 5. The total positive circulation associated with one wingbeat, normalized by Γ_1, the reference circulation required for nominal weight support. Symbols as figure 3.

downstroke. Just adding the circulation to the total for the downstroke structure exaggerates its effect. However, here, the purpose of the measurement is for an approximate check on the sufficiency of the force balance only, and the added operational convenience (a consideration for an extensive survey of all flight speeds for two individuals) is quite considerable as each vorticity field requires only two passes, and not four as in Spedding *et al.* (2003*b*). In making the calculation this way, we look especially for $|\Gamma_{tot}|/\Gamma_1=1$ at low speeds ($U=4\,\mathrm{m\,s^{-1}}$), if the measured wake contains sufficient vertical impulse. Thereafter, as U increases, one expects $|\Gamma_{tot}|/\Gamma_1$ to increase above one. The result is shown in figure 5 and $|\Gamma_{tot}|/\Gamma_1\approx 1$ for $U\leq 6\,\mathrm{m\,s^{-1}}$. As another consistency check, one expects that $\Gamma^+_{tot}+\Gamma^-_{tot}=0$, at all flight speeds, and this is seen in figure 5.

For higher values of U, the assumptions of the procedure become increasingly unrepresentative of the true structure of the wake. Furthermore, the vertical centreplane circulation estimates through cross-stream or spanwise vortex structures are not clearly related to the magnitude of the trailing, streamwise vortices, whose presence can be inferred by the spanwise population of vertical plane measurements, but whose magnitude cannot easily be measured.

3.4. Wing kinematics

Since the flapping wings are the source of the wake vortices, an interpretation of the wake pattern can be connected with the wing movements. Following Rosén *et al.* (2004), some basic kinematic measures were obtained from high speed video sequences of bird#1 across the speed range $U=4$–$9\,\mathrm{m\,s^{-1}}$ (figure 6). The wingbeat frequency ranged between 14.1 and 15.5 Hz, rising slightly with increasing U, but the trend is not statistically significant (figure 6*a*; ANOVA, $F_{5,28}=1.30$, $p>0.05$). The wing tip peak–peak amplitude, A, increased from 0.10 m at $U=4\,\mathrm{m\,s^{-1}}$ to 0.14 m at $U=9\,\mathrm{m\,s^{-1}}$ (figure 6*b*; ANOVA, $F_{5,28}=17.63$, $p<0.001$). Downstroke fraction, τ, remained within the range 0.44–0.49 with no significant variation among speeds (figure 6*c*; ANOVA, $F_{5,28}=1.75$, $p>0.05$). The span ratio, R, varied from 0.33 ± 0.02 at $U=4\,\mathrm{m\,s^{-1}}$ to maximum 0.49 ± 0.02 at $U=9\,\mathrm{m\,s^{-1}}$, which is a significant change across the speed range (figure 6*d*; ANOVA, $F_{5,28}=3.83$, $p<0.01$). The reduced frequency, k, was maximum 1.05 at $U=4\,\mathrm{m\,s^{-1}}$, and then declined with increasing speed to 0.51 at $U=9\,\mathrm{m\,s^{-1}}$ (figure 6*e*), largely because it is inversely proportional to flight speed while the wingbeat frequency is constant.

4. DISCUSSION

4.1. Wake topology

This study is the second to apply quantitative DPIV techniques to birds in wind tunnel flight. The instantaneous velocity and vorticity fields taken at various plane sections in the wake show the footprint caused by the bird and its wingbeat, and one may compare wakes between species to see what (if any) measurable differences in the footprint reflect differences in the morphology and kinematics.

Qualitatively, the wakes of the robin and thrush nightingale are indistinguishable (figure 1 may be compared with figures 8 and 14*a* in Spedding *et al.* 2003*b*). They both show compact start vortices and more diffuse stop vortices when measured in cross-section. Both show a gradually, increasingly evident wake signature on the upstroke part of the wake as the flight speed increases.

Quantitatively, the continuous decrease in strength of the wake structures measured in the vertical centreplane (figure 2, and fig. 25 in Spedding *et al.* 2003*b*), as measured by Ω^+ and Ω^- and Γ^+ and Γ^- is similar in shape for the two species, showing the same gradual transition from slow speed to high-speed flight. At $U=4\,\mathrm{m\,s^{-1}}$, $\Gamma^+=1.2$ for the thrush nightingale and 1.1 for the robin. The thrush nightingale and the robin differ very little in basic morphology, except the robin body mass is about half of that in the thrush nightingale, and so the wing loading, Q, is significantly lower. It is useful to enquire how this might be expected to affect the measured Γ in the wake.

One might ask: for similar flying devices, how would Γ/Uc vary with U and with Q? Let us begin with the simplest possible flight model (see any standard aerodynamics text, such as Anderson 1984) where the Kutta–Joukowski lift per unit span of a body moving at uniform speed, U, and with circulation Γ is

$$L' = \rho\Gamma U. \tag{4.1}$$

Therefore, for a wing of finite span, $2b$, the total lift is

$$L = \rho 2b\Gamma U, \tag{4.2}$$

if all finite-span effects are ignored. As a rough approximation, this is easily adequate for our current level of detail. In steady flight, $L=W$, and so equation (4.2) can be re-arranged slightly to give

$$\Gamma = \frac{W}{\rho 2bU} = \frac{Wc}{S\rho U}, \tag{4.3}$$

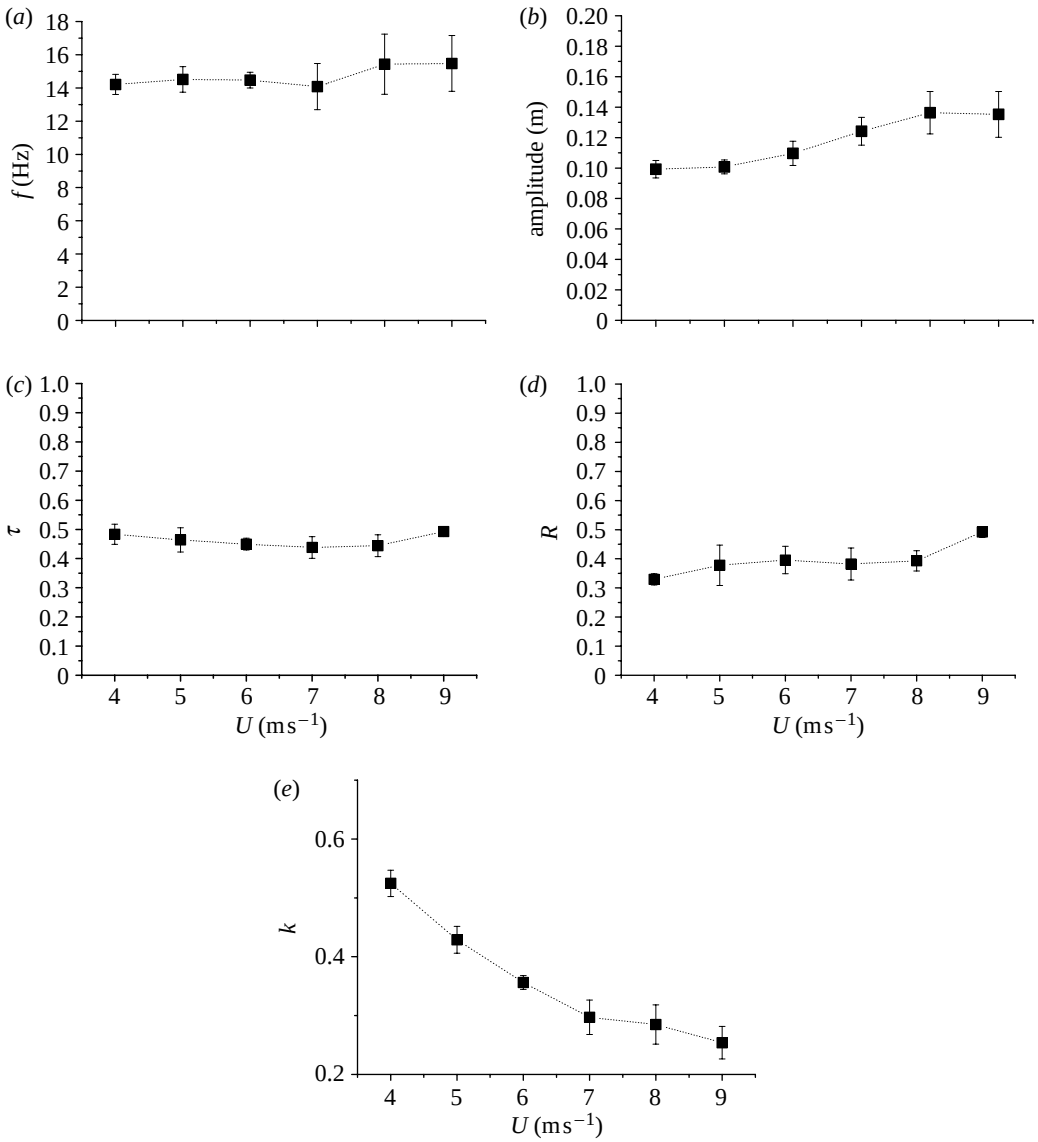

Figure 6. Wingbeat kinematics of robin #1 as a function of flight speed U. (a) Wing beat frequency, (b) amplitude, (c) downstroke fraction, (d) wing span reduction at mid upstroke in relation to mid downstroke, (e) reduced frequency, k. The number of sequences analysed for each speed were [6, 7, 6, 5, 8, 2] for U=[4, 5, 6, 7, 8, 9] m s^{-1}, respectively.

where $S=2bc$ is the wing planform area, and c is the mean chord. Equation (4.3) predicts Γ for all flight speeds U, for any bird whose morphology is given by the body mass, m (and hence $W=mg$), and wing planform geometry b and c.

Table 2 collects data from the literature for all cases where Γ has been measured in the wake, and for which these minimal morphological parameters are also known. Equation (4.3) is then run numerically, and the result is given in figure 7. The continuous curves are the predicted values of Γ that should be measured in the wake of each bird over a range of U from 2 to 13 m s^{-1}. Existing experimental data are shown as symbols. Given the broad assumptions, the agreement is quite good, and, given the broad assumptions, one might wonder why this is, particularly when these same circulation measurements have only 50% of the magnitude required for weight support from the elliptical loop model. Interestingly, equation (4.2) implicitly maps out a steady self-propelled wake that provides weight support over the entire area traced by the wings, and it is exactly equal to equation (2.8), introduced as a reference circulation for the ideal steady powered glider. Even though the real wakes are being generated in pulses, with most activity in the downstroke (particularly at low speeds), the (uncorrected) measured circulation of the coherent wake structures is roughly equal to that expected from the ideal powered wake as if it were continuous, not pulsed.

Comparatively, the furthest data point from the predicted curves is for the kestrel wake, which is the only circulation measurement to come from the cross-stream (y, z) plane, so the higher measured circulation derives from sections through the trailing vortices. Its value in figure 7 is higher than the curve because the real undulating wake has a smaller horizontal projected area than the implicitly assumed rectangle between constantly outstretched wingtips. When this wake geometry is correctly taken into account, the vertical impulse matches exactly that required to support the weight, as shown in Spedding (1987*a*).

JOURNAL OF THE ROYAL SOCIETY Interface
JOURNAL OF THE ROYAL SOCIETY Interface

Table 2. Morphology and wake properties compiled from wake visualization studies of bird flight. (AR is aspect ratio, Q is wing loading, f is wing beat frequency, U is flight speed, R_0 is vortex core radius, R is vortex ring radius, ω is vorticity, c is mean wing chord, b is semispan, Γ is circulation, I is impulse, T is time period, m is body mass, g is acceleration due to gravity.)

species[a]	m (kg)	b (m)	c (m)	AR	Q (N m^{-2})	f (Hz)	U (m s^{-1})	topology	R_0/R	$\omega_{\max}c/U$	Γ/Uc	I/Tmg[b]	source
pigeon	0.35	0.33	0.094	7.0	55.9	6.7	2.4	loop	0.17	18.8	7.63	0.52[c]	Spedding *et al.* (1984)
jackdaw	0.216	0.296	0.095	6.0	38.2	5.6	2.5	loop	0.14	4.54	3.47	0.35[c]	Spedding (1986)
kestrel, downstroke	0.21	0.338	0.076	8.8	39.6	7.7	7	cc	0.097[d]	1.80	0.94	1.04[e]	Spedding (1987*a*)
kestrel, upstroke	0.21	0.338	0.076	8.8	39.6	7.7	7	cc	0.39[d]	0.55	1.13		Spedding (1987*a*)
thrush nightingale	0.030	0.131	0.048	5.4	23.6	14.4	4	loop	0.11	8.7	1.28	0.45[c]	Spedding *et al.* (2003*b*)
							7	loop-cc		2.2	0.45	0.5[c]	Spedding *et al.* (2003*b*)
							10	cc		0.8	0.15	0.72[e]	Spedding *et al.* (2003*b*)
robin, 2 birds	0.0165	0.11	0.047	4.7	15.6	14.8	4	loop	0.16	4.18	1.06	0.50[c]	this study
							6	loop-cc		2.94	0.50	0.50[c]	this study
							9	cc		0.98	0.17	1.07[e]	this study
kestrel, gliding	0.21	0.338	0.076	8.8	40.0	0	7	cc-glide	0.2[d]	0.99	0.93	1.04[e]	Spedding (1987*b*)

[a] Scientific names: pigeon *Columba livia*, jackdaw *Corvus monedula*, kestrel *Falco tinnunculus*, thrush nightingale *Luscinia luscinia*, robin *Erithacus rubecula*.
[b] This quantity denotes sufficiency of supporting the weight when $I/Tmg \geq 1$.
[c] In relation to reference circulation $\Gamma_1 = mgT/\rho S$ (see text for symbol definitions).
[d] Core radius in relation to transverse distance between wing tip vortices.
[e] In relation reference circulation $\Gamma_0 = mg/\rho U 2b$ (see text for symbol definitions).
[f] Refers to an aggregated vortex in a confined space, not the result of a single downstroke.

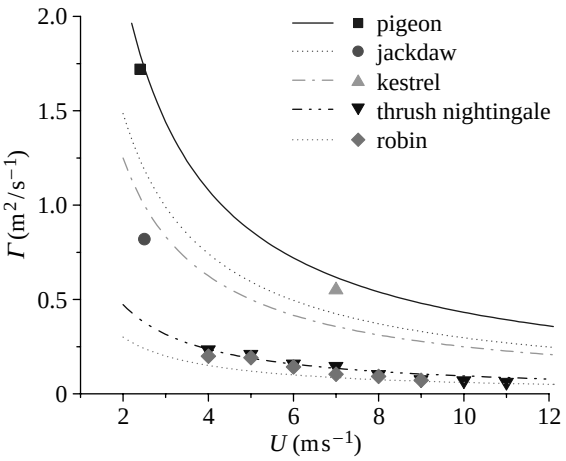

Figure 7. Predicted (continuous lines) and measured (symbols) circulations for five bird species for whom wake data are available. The lines come from equation (4.3), derived only from the continuous circulation required for lift in a steady uniform potential flow. Data are from Spedding *et al.* (1984, 2003*b*), Spedding (1986, 1987*a*) and this study.

From a practical point of view, the dimensional circulation measured in any bird wake ought to be predictable by equation (4.3). The normalized circulation is

$$\frac{\Gamma}{Uc} = \frac{W}{S}\frac{1}{\rho U^2}. \tag{4.4}$$

Γ/Uc varies with U^{-2} and directly with $W/S = Q$, the wing loading. That is why the thrush nightingale with its higher wing loading, occupies a higher curve in figure 7 (or normalized equivalent) than the robin. Also note that equation (4.4) can be written using the dynamic pressure, $q = (1/2)\rho U^2$, as

$$\frac{\Gamma}{Uc} = \frac{W}{S2q} = \frac{Q}{2q}. \tag{4.5}$$

The simplicity of this prediction is again striking: the predicted circulation of bird wake structures depends on the ratio of wing loading (force per unit area), Q, to dynamic pressure (force due to mass flux per unit area), q. All other things being equal, the wing geometry and body size and density determine Q, and the flight speed then determines q.

4.2. Wing kinematics

Just as the wake comparisons proved instructive, so we can summarize the wingbeat kinematics of the two birds for which there are comprehensive wake data over a continuous range of U. Figure 8 shows the result, simplified with fitted curves to show only the main trends. In figure 8*a* the wing beat frequency is shown to rise very slightly with flight speed (note the small scale range in f). Pennycuick (1996) derived a dimensionally correct equation to predict wing beat frequency in flapping flight on the basis of body mass, wing span, wing area, acceleration due to gravity and air density, which gives constant values of 12.3 and 12.1 Hz for the robin and thrush nightingale, respectively. These are shown as horizontal lines in figure 8*a*. The observed mean frequencies were 14.7 and 14.4 Hz. Predicted and observed differences between the species in wing beat frequencies are thus very similar, even though the thrush nightingale is almost twice as heavy as the robin, but the observed frequencies were higher than predicted. An alternative formula to calculate the wingbeat frequency was recently derived by Nudds *et al.* (2004). For $U = 9\ \mathrm{m\ s^{-1}}$ this formula yields 12.8 and 10.0 Hz for the robin and thrush nightingale, respectively.

There are some indications that swallows flying in a wind tunnel exhibit elevated wing beat frequency compared with freely migrating birds (Liechti & Bruderer 2002), but that study compared juvenile birds of shorter wings with adult birds on spring migration with unknown weight differences. The natural range of wing beat frequency in small passerines is 12–18 Hz (Bruderer 1971; Bäckman & Alerstam 2003), and the robin and nightingale fall in the middle of this range. Radar echo-signatures of released robins flying intermittently with a flapping ratio = 0.82 showed an average wingbeat frequency of 15.2 Hz (Stark 1996), i.e. somewhat higher than the wind tunnel birds. It should be noted that the wind tunnel flights invariably refer to continuous flapping flight.

The graphs of $f(U)$, $\tau(U)$ and $R(U)$ are very similar between the two species. In the thrush nightingale kinematic data, the primary variation with flight speed U was a small decrease in τ, and a commensurate increase in R. This is consistent with the qualitative wake patterns showing the increased importance of the upstroke, as the wing is extended further from the body (R) and for a comparatively longer time (τ). The principal difference between the two bird species is in wingbeat amplitude, which rises with increasing U in the robin, and not in the thrush nightingale. If an ER-type flight model (Spedding *et al.* 2003*b*) is equally correct for both species, and the data suggest this is so, then an increased amplitude wake will translate to a larger thrust at a given speed, implying a larger drag. We cannot claim sufficient resolution of all wake features in three-dimensional to go beyond this conjectural stage, but an example of the type of calculation involved will be given in the following section.

A simple connection can be made between wake and wingstroke kinematics. Recalling equation (4.3), which relates the required circulation to the morphology and flight speed as

$$\Gamma = \frac{Wc}{\rho S U},$$

we can introduce the reduced frequency to describe the dependence on $1/U$, so since

$$k = \frac{\pi f c}{U}$$

equation (4.3) becomes

$$\Gamma = \frac{W}{S}\frac{k}{\rho \pi f}. \tag{4.6}$$

Since the flapping frequency, f, is approximately constant, then the denominator $\rho\pi f$ is constant and

$$\Gamma \propto Qk. \tag{4.7}$$

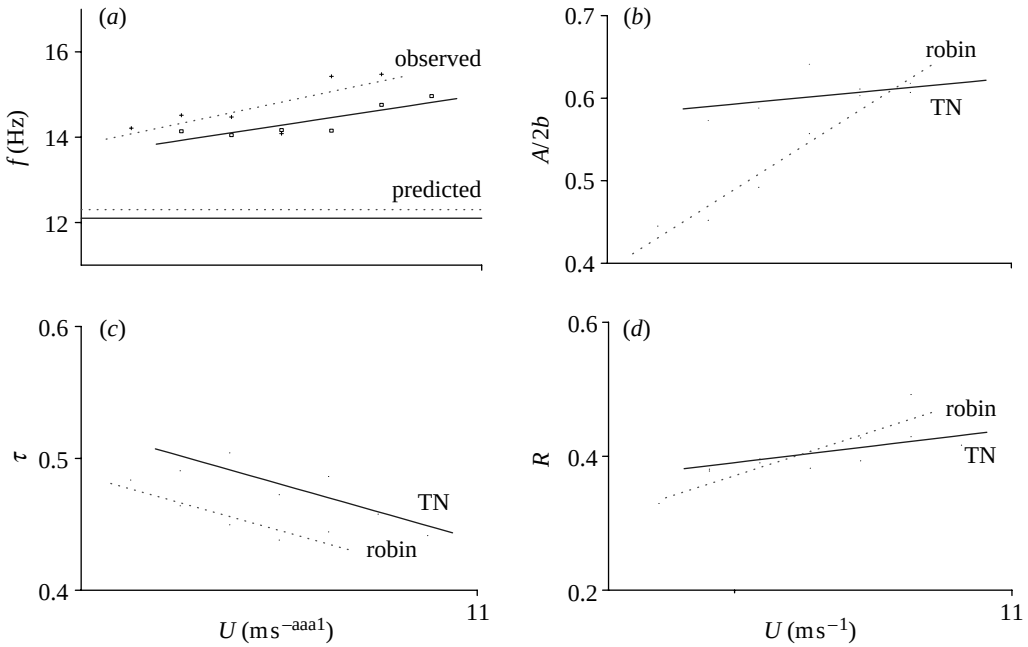

Figure 8. A simple summary of kinematic data as a function of flight speed, U, for the thrush nightingale (solid blue) and robin (dotted red), both measured in similar wind tunnel experiments. The panels show wing beat frequency (Hz), normalized wingbeat amplitude, downstroke ratio and span ratio in (a–d). The data are shown only by the least squares linear fit line, except for $f(U)$ in (a) where individual points are given as an example of the scatter around the fit. Figure 6 may be consulted for further details in the robin data.

The (dimensional) circulation observed in the wake should be directly proportional to the wing loading, Q, and to the reduced frequency, k. Either equation (4.3) or (4.6) could be used to predict measured circulations for birds at equivalent flight speeds, where the wake geometry is sampled similarly.

Alternatively, for an as-yet unmeasured bird, then equation (4.6) can be recast as

$$\Gamma_{\mathrm{obs}} = CQ\frac{k}{f}, \tag{4.8}$$

where $C = 1/(\rho\pi) \cong 1/\pi \cong 1/3$. Γ_{obs} is the value that is predicted to be observed in the strong start vortices in the wake.

Finally, we may also note that since $|\omega_y|_{\max} \propto \Gamma$ (figure 2) and $\Gamma \propto Qk$ (equation (4.7)), then we expect also $|\omega_y|_{\max} \propto Qk$. Alternatively, if the bird morphology is known, then equation (4.3) can be used directly,

$$|\omega_y|_{\max} \propto \frac{Wc}{\rho SU}. \tag{4.9}$$

4.3. Force balance

Previous quantitative vortex wake studies at slow speeds ($U \leq 4\ \mathrm{m\,s^{-1}}$) showed that approximately half (or less) of the momentum required to support the weight could be derived from the circulation confined to the strongest start vortex at slow speeds (Spedding *et al.* 1984, 2003*b*; Spedding 1986). This result was repeated also in this study of robins at $U = 4\ \mathrm{m\,s^{-1}}$, with near 50% of the circulation required to support the weight confined to the main start vortex. The wake vorticity distribution was very similar to that of the thrush nightingale, studied under identical conditions, with asymmetric vortex loops at slow speeds, $U = 4$–$5\ \mathrm{m\,s^{-1}}$, in the sense that the stronger start vortex has a smaller cross-section than the more diffuse stop vortex. The stop vortex with negative (clock-wise) circulation has within its neighbourhood, broad-spread low amplitude vorticity of positive circulation. This weak but widespread positive circulation must be added to that of the strong starting vortex so that enough circulation could be recovered in the wake to claim weight support at slow speed, i.e. the measured circulation is reasonably close to the reference circulation Γ_1.

It is not clear why the wake vorticity is spread out this way. It is possible that the wake deforms under its own induced velocity field in the time elapsed between formation and measurement. It is possible that the wings, tail and body of the bird interfere with the near wake and complicate its structure. It is also possible that some of these interference effects are actually deliberate, where energy to maintain a preferred flow over the wings is reclaimed from the wake itself. However, given the complications in accounting for all wake components (whatever their cause), it appears that the vertical forces are in satisfactory balance.

The vertical component of the aerodynamic force, L, is significantly larger than the horizontal component, which is the thrust required to balance the aerodynamic drag, D, of the bird. In mechanical models of bird flight the drag is estimated at different speeds and then multiplied by speed to obtain mechanical power, P, which is plotted against flight speed, U (Pennycuick 1975, 1989*b*). From such curves it is possible to identify characteristic speeds for minimum power and maximum range, the latter being associated with maximum L/D and an optimal cruising speed in migrating birds (Pennycuick 1969; Hedenström & Alerstam 1995).

Ideally, by knowing the wake topology and its associated circulation it might be possible to calculate the net horizontal force and generate $P(U)$-relations from wake information alone.

It is important to note that such an enterprise can work if, and only if, the lift- and thrust-producing wake can be separated from the viscous drag wakes shed by the wings and body. As noted in Spedding *et al.* (2003*b*), the net horizontal momentum flux of a self-propelled body in unaccelerated horizontal motion is exactly zero. In order to claim any measurement of net thrust or drag in the wake, it must be possible to separate out the different components. It was remarked in Spedding (1987*a*) that viscous drag wakes clearly marked the cores of trailing vortices in kestrel wakes, and in Spedding *et al.* (2003*b*) drag wakes from wings and tail/body were identified from selections where the bird was gliding. The complex patterns of figure 1 do not encourage strong hopes of being able to separate thrust and drag wake components—partly because the wake is comparatively far from its point of origin. In order to make progress and at least illustrate the concept, we must make rather strong assumptions about the wake structure and its measurement, which might take the following form.

Let us suppose that the drag wake occurs in the form of a velocity defect in the cores of vortices that trace out some kind of wake structure. Suppose that the drag force that this represents is balanced by a net thrust that occurs because (simplifying a little) the downstroke wake is larger than the upstroke wake, and the difference in projected areas of the wakes gives the net rearward momentum flux that balances the net drag. Now, the thrust and drag wake components can be considered as separable, and the magnitude of the thrust (equal to the drag) can be estimated from the wake geometry and circulation, as if the viscous drag did not contribute (the drag wake is confined to vortex cores of the global wake geometry, whose overall asymmetry provides the thrust).

Spedding *et al.* (2003*b*) presented a conceptual model based on a wake consisting of downstroke elliptic loops and upstroke rectangular vortices (ER-model). The relative circulation between upstroke and downstroke is controlled by a factor, C_{u}, which when equal to zero means the upstroke is aerodynamically unloaded and when equal to one is a wake of constant circulation throughout the wingbeat cycle. The net horizontal impulse from one downstroke and one upstroke, based on the geometry of the wake and kinematics of the wingbeat can be written as

$$I_x = \rho b h \Gamma_{\mathrm{d}} \left(\frac{\pi}{2} - 2 C_{\mathrm{u}} R \right), \tag{4.10}$$

where ρ is air density, b is semi-span, h is wake height, Γ_{d} is downstroke circulation and R is the span ratio (see Spedding *et al.* 2003*b* for further details). From I_x the associated thrust is given by $F_x = I_x / T$, where T is the wingbeat period. If the measurement of Γ_{d} is unaffected by the presence of the drag component of the wake, then equation (4.10) gives a calculation of the thrust component only of F_x.

To claim an accurate calculation of F_x across the entire speed range is perhaps unrealistic since the calculation would mainly reflect the uniformity of untested assumptions in the force component separation criteria. However, mainly as an illustrative example, we made one calculation for $U = 9\ \mathrm{m\ s^{-1}}$, where the wake topology is sufficiently simple and the measured circulations are similar between downstroke and upstroke. For the morphology of the robin (table 1), a wake height of $h = 0.135$ m, wingbeat period $T = 0.065$ s, span ratio $R = 0.49$ (figure 5), $C_{\mathrm{u}} = 0.8$ and $\Gamma_{\mathrm{d}} = 0.1\ \mathrm{m^2\ s^{-1}}$, one arrives at $F_x = 0.022$ N and $L/D = 7.5$. Because the exact details of the wake topology at slow speeds are still difficult to interpret it would be potentially misleading to calculate L/D across the entire speed range to determine, e.g. the optimal cruising speed. The calculation given here for $U = 9\ \mathrm{m\ s^{-1}}$ should also be considered as provisional.

In gliding birds L/D is determined by the point on the glide polar where the ratio between forward and sink speed, U/U_z, is maximum. In a Harris' hawk *Parabuteo unicinctus* L/D was estimated at 11.6 (Tucker & Heine 1990) and in a jackdaw it was 12.6 (Rosén & Hedenström 2001). The higher values in gliding flight compared to the robin in flapping flight are likely due to higher aspect ratio wings in the gliders, but may yet point to a higher aerodynamic efficiency in gliding flight.

Since $P = DU$, the effective $L/D = mgU/P$, where P is mechanical power, and so in principle P can be derived from measured values of D, when the condition, $L = W$ is known to apply. Other methods of estimating P from birds flying in wind tunnels have been either measures of muscle shortening and lengthening to obtain work loops, or measures of metabolic power input by the use of respirometry or doubly labelled water, coupled with an assumption about the conversion efficiency of chemical energy to mechanical work (Biewener 2003). From studies using the work loop approach one may estimate an effective $L/D = 9$ in the starling *Sturnus vulgaris* (Biewener *et al.* 1992), $L/D = 8$ in the pigeon *Columba livia* (Dial & Biewener 1993) and $L/D = 10$ in the magpie *Pica pica* (Dial *et al.* 1997). Estimates of effective L/D based on respirometry (assuming the customary constant conversion efficiency of 0.23) range from about 4 in the budgerigar *Melopsittacus undulatus* (Tucker 1968) to 14 in the bar-headed goose *Anser indicus* (Ward *et al.* 2002). The broad range of values derived from respirometry experiments probably reflects the additional uncertainties in experimental conditions and the extra layer of assumptions required to convert chemical energy to mechanical work. Overall $L/D = 7.5$ for the robin seems as plausible as any other estimate, but just like all the other estimates, it lacks an independent alternative measure. Experiments measuring the wakes of steady gliding birds are planned.

5. CONCLUDING REMARKS

The wakes of two individual robins have been measured under identical conditions, and quantitative measures of vorticity and circulation were indistinguishable between the two birds. In experiments that have a physical model that parameterizes measured individual differences (e.g. wing span, body mass, wing loading)

there is no reason to expect any significant variation between calculated values between the individuals. The forces must balance for each bird, not for a statistical average of a population, which was the case here, within measurement uncertainty. There is more to gain from studying other species of differing morphology rather than enlarged samples of already studied species.

The quantitative properties of the wake vortices turned out to be well-predicted by a very simple flight model that makes no assumptions at all about the pulsed, non-uniform character of the real wake. The close agreement was achieved not only for the robin and thrush nightingale data, but for all existing quantitative wake data in the literature. Some simple manipulations of this model allowed expressions to be written to predict, for example, measured circulations of start vortices in future bird flight experiments.

The wake vortices were measured some 17 chord lengths downstream from the bird. Even though the wakes are consistent with hypothesized models (Spedding *et al.* 2003*b*), they also exhibit complexities that may arise between shedding at the wing and time of recording. The effect of the evolution of the wake can best be understood by closing the distance between the bird and imaging location, and plans are in place to do that. A closer investigation of the steady and unsteady aerodynamics around the wings themselves will be assisted by companion experiments on simple fixed wing models. A complete characterization of near-wake dynamics (inviscid and vortical) will likely require the use of fully three-dimensionally resolved DPIV. Then one might also directly estimate the net horizontal forces over a wingbeat, which will be required to generate a true *wake-based* $P(U)$-curve.

We are grateful for the support of C. J. Pennycuick and T. Alerstam throughout this project and the comments by two anonymous referees. The research was supported by the Knut and Alice Wallenberg foundation, the Carl Tryggers foundation, the Swedish Research Council and the Swedish Foundation for International Cooperation in Research and Higher Education (STINT) (to A. H). A. H. is a Royal Swedish Academy of Sciences Research Fellow supported by a grant from the Knut and Alice Wallenberg Foundation. This study was approved by the Lund University Ethical committee for the use of live animals in research and follows the legal requirements in Sweden for keeping animals in captivity for research purposes.

REFERENCES

Anderson, J. D. 1984 *Fundamentals of aerodynamics*. New York: McGraw-Hill.

Bäckman, J. & Alerstam, T. 2003 Orientation scatter of free-flying nocturnal passerine migrants: components and causes. *Anim. Behav.* **65**, 987–996. (doi:10.1006/anbe.2003.2119)

Biewener, A. A. 2003 *Animal locomotion*. Oxford: Oxford University Press.

Biewener, A. A., Dial, K. P. & Goslow, G. E. 1992 Pectoralis muscle force and power output during flight in the starling. *J. Exp. Biol.* **164**, 1–18.

Bruderer, B. 1971 Radarbeobachtungen über den Frühlingszug im schweizerischen Mittellan. *Orn. Beob.* **68**, 89–158.

Dial, K. P. & Biewener, A. A. 1993 Pectoralis muscle force and power output during different modes of flight in pigeons (*Columba livia*). *J. Exp. Biol.* **176**, 31–54.

Dial, K. P., Biewener, A. A., Tobalske, B. W. & Warrick, D. R. 1997 Mechanical power output of bird flight. *Nature* **390**, 67–70. (doi:10.1038/36330)

Fincham, A. M. & Spedding, G. R. 1997 Low-cost, high resolution DPIV for measurement of turbulent fluid flow. *Exp. Fluids* **23**, 449–462. (doi:10.1007/s003480050135)

Hedenström, A. & Alerstam, T. 1995 Optimal flight speed of birds. *Phil. Trans. R. Soc. B* **348**, 471–487.

Liechti, F. & Bruderer, L. 2002 Wingbeat frequency of barn swallows and house martins: a comparison between free flight and wind tunnel experiments. *J. Exp. Biol.* **205**, 2461–2467.

Nudds, R. L., Taylor, G. K. & Thomas, A. L. R. 2004 Tuning of Strouhal number for high propulsive efficiency accurately predicts how wingbeat frequency and stroke amplitude relate and scale with size and flight speed in birds. *Proc. R. Soc. B* **271**, 2071–2076. (doi:10.1098/rspb.2004.2838)

Pennycuick, C. J. 1969 The mechanics of bird migration. *Ibis* **111**, 525–556.

Pennycuick, C. J. 1975 Mechanics of flight. In *Avian biology* (ed. D. S. Farner & J. R. King), vol. 5, pp. 1–75. New York: Academic Press.

Pennycuick, C. J. 1989*a* Span-ratio analysis used to estimate effective lift:drag ratio in the double-crested cormorant *Phalacrocorax auritius* from filed observations. *J. Exp. Biol.* **142**, 1–15.

Pennycuick, C. J. 1989*b* *Bird flight performance: a practical calculation manual*. Oxford: Oxford University Press.

Pennycuick, C. J. 1996 Wingbeat frequency of birds in steady cruising flight: new data and improved predictions. *J. Exp. Biol.* **199**, 1613–1618.

Pennycuick, C. J., Alerstam, T. & Hedenström, A. 1997 A new low-turbulence wind tunnel for bird flight experiments at Lund University, Sweden. *J. Exp. Biol.* **200**, 1441–1449.

Rayner, J. M. V. 1979*a* A vortex theory of animal flight. Part 2. The forward flight of birds. *J. Fluid Mech.* **91**, 731–763.

Rayner, J. M. V. 1979*b* A new approach to animal flight mechanics. *J. Exp. Biol.* **80**, 17–54.

Rosén, M. & Hedenström, A. 2001 Gliding flight in a jackdaw: a wind tunnel study. *J. Exp. Biol.* **204**, 1153–1166.

Rosén, M., Spedding, G. R. & Hedenström, A. 2004 The relationship between wingbeat kinematics and vortex wake of a thrush nightingale. *J. Exp. Biol.* **207**, 4255–4268. (doi:10.1242/jeb.01283)

Spedding, G. R. 1986 The wake of a jackdaw (*Corvus monedula*) in slow flight. *J. Exp. Biol.* **125**, 287–307.

Spedding, G. R. 1987*a* The wake of a kestrel (*Falco tinnunculus*) in flapping flight. *J. Exp. Biol.* **127**, 59–78.

Spedding, G. R. 1987*b* The wake of a kestrel (*Falco tinnunculus*) in gliding flight. *J. Exp. Biol.* **127**, 45–57.

Spedding, G. R. 1992 The aerodynamics of flight. In *Advances in comparative and environmental physiology. The mechanics of animal locomotion* (ed. R. McN. Alexander), pp. 51–111. Berlin: Springer.

Spedding, G. R., Rayner, J. M. V. & Pennycuick, C. J. 1984 Momentum and energy in the wake of a pigeon (*Columba livia*) in slow flight. *J. Exp. Biol.* **111**, 81–102.

Spedding, G. R., Hedenström, A. & Rosén, M. 2003*a* Quantitative studies of the wakes of freely-flying birds in a low-turbulence wind tunnel. *Exp. Fluids* **34**, 291–303. (doi:10.1007/s00348-002-0559-8)

Spedding, G. R., Rosén, M. & Hedenström, A. 2003*b* A family of vortex wakes generated by a thrush nightingale in free

flight in a wind tunnel over its entire natural range of flight speeds. *J. Exp. Biol.* **206**, 2313–2344. (doi:10.1242/jeb.00423)

Stark, H. 1996 Flugmechanik nachts ziehender Kleinvögel. Ph.D. thesis, Basel University.

Tucker, V. A. 1968 Respiratory exchange and evaporative water loss in the flying budgerigar. *J. Exp. Biol.* **48**, 67–87.

Tucker, V. A. & Heine, C. 1990 Aerodynamics of gliding flight in a Harris' hawk, *Parabuteo unicinctus*. *J. Exp. Biol.* **149**, 469–489.

Ward, S., Bishop, C. M., Woakes, A. J. & Butler, P. J. 2002 Heart rate and the rate of oxygen consumption of flying and walking barnacle geese (*Branta leucopsis*) and bar-headed geese (*Anser indicus*). *J. Exp. Biol.* **205**, 3347–3356.